MILCOM 2024 - 2024 IEEE Military Communications Conference (MILCOM) | 979-8-3503-7423-0/24/$31.00 ©2024 IEEE | DOI: 10.1109/MILCOM61039.2024.10773683

Sidelink-Enabled Cooperative Localization for xG Non-Terrestrial Networks

James C. Morrison*, Nathan Schatz*, Seungnyun Kim*, Girim Kwon*, Bernardo Camajori Tedeschini*, Vijitha Weerackody‡, Andrea Conti§, and Moe Z. Win††

*Wireless Information and Network Sciences Laboratory, Massachusetts Institute of Technology, Cambridge, MA, USA
‡Applied Physics Laboratory, Johns Hopkins University, Laurel, MD, USA
§Department of Engineering and CNIT, University of Ferrara, Ferrara, Italy
††Laboratory for Information and Decision Systems, Massachusetts Institute of Technology, Cambridge, MA, USA

***Abstract*—Location awareness is essential for next-generation (xG) network capabilities, including satellite-terrestrial integration, adaptive beamforming, and vehicle-to-everything (V2X) scenarios. The recent proliferation of low Earth orbit (LEO) satellites offers a high signal-to-noise ratio (SNR) alternative to global navigation satellite systems (GNSSs) for positioning, navigation, and timing (PNT) in mobile ground terminals. However, the timing drift of LEO clocks complicates the localization problem by introducing clock offset variables into the parameter vector used for location inference. Conventional PNT approaches are rigid in their requirements for LEO non-terrestrial network (NTN) size and access to gNodeB (gNB) base stations (BSs). Others relax these constraints and suffer from substantial localization errors and refine the estimate through filtering over time. This paper presents the theoretical foundation for joint cooperative localization and synchronization (JCLS) using time-of-arrival (TOA) measurements from both downlink (DL) and sidelink (SL) signals. System performance simulation results demonstrate meter-level 3-dimensional positioning, highlighting the potential of the proposed approach for robust and efficient localization in challenging electromagnetic environments.**

***Index Terms*—PNT, localization, cooperation, non-terrestrial network, sidelink.**

I. Introduction

Location awareness is crucial for next-generation (xG) networks. In the 3rd Generation Partnership Project (3GPP) Release (Rel)-18, quality of service requirements are specified for various 5G location services (LCS), from 10 m–50 m for navigation to 200 km for weather reports and warnings [1]. In Rel-19, additional location awareness scenarios are considered: the corresponding service level requirements (PSLs) are between 0.2 m for relative positioning between user equipments (UEs) and 10 m for indoor and outdoor positioning [2], [3]. These key performance indicators are designed to enhance user mobility and support higher density in scenarios such as industrial automation, unmanned aerial vehicle control, augmented reality, and public safety. Furthermore, location awareness will be required to realize xG capabilities like uplink (UL) frequency correction for non-terrestrial network (NTN) access [4], adaptive beamforming [5], vehicle-to-everything (V2X) scenarios [6]. It is also critical for enabling low probability of intercept/detection (LPx) communications and Joint All Domain Command and Control (JADC2) for the Department of Defense (DoD), particularly by contributing rapid sensing in degraded and contested electromagnetic environments [7].

Modern technologies rely on access to global navigation satellite systems (GNSSs) for positioning, navigation, and timing (PNT). GNSS satellites transmit a direct-sequence spread spectrum (DSSS) reference signal to perform time-of-arrival (TOA) localization from medium Earth orbit (MEO) and geostationary Earth orbit (GEO), resulting in weak receive powers that are susceptible to interference, jamming, and harsh propagation environments [8], [9]. Since the advent of low Earth orbit (LEO) megaconstellations like Starlink, Orbcomm, OneWeb, and Iridium, abundant downlinks (DLs) are available as signals of opportunity for localization that have 24–34 dB (about 250–2,500 times) higher signal-to-noise ratio (SNR) than those from MEO [10]. However, PNT with LEO satellites is hard because, unlike GNSS atomic clocks, the LEO ultra-stable oscillators and oven-controlled crystal oscillators fail to provide precise timing required for localization, despite supporting high-throughput communications [11]. When modeled as unknown parameters, the clock offsets of each satellite cause the observation model to be underconstrained, regardless of the number of satellites available. Therefore, a new parameter has to be estimated at each measurement.

Previous efforts on PNT via LEO satellites have been directed towards collating time-disparate measurements before estimation or combining reference signals from LEO satellites and terrestrial anchors. In such cases, the localization problem has been formulated as a tracking problem using various permutations of the time, frequency, and carrier phase of arrival measurements. One strategy filters pseudoranges, accumulated DL Doppler shifts, and an inertial measurement unit (IMU) [12]. Another uses a base-rover paradigm to perform precise positioning using carrier phase measurements [13]. Due to the nature of the tracking problem, many system models assume GNSS access before the navigation scenario begins [12]. Furthermore, carrier phase methods require the presence of a terrestrial base station (BS), which is insufficient for PNT at

The fundamental research described in this paper was supported, in part, by the Office of Naval Research under Grant N62909-22-1-2009, by the National Science Foundation under Grant CNS-2148251, and by federal agency and industry partners in the RINGS program. *Corresponding author: Moe Z. Win (e-mail: moewin@mit.edu).*

remote UEs [13]. Models which require neither GNSS nor BSs are often rigid in their requirements for satellite availability; for example, the Doppler model requires 8 satellites to localize UEs [14]. Finally, models which only use LEO reference signals and are flexible in satellite requirements demonstrate slow estimation convergence; for example, a minute to reach 200 m accuracy [15]. Current literature is missing contributions to rapidly provide accurate position estimates for variable-size NTNs when GNSS and gNodeB (gNB) BSs are not available.

Spatiotemporal cooperation has been used to improve localization accuracy in wireless networks [16]. In the context of PNT with LEO satellites, the use of a sidelink (SL) between UEs would enable cooperation through measurement sharing. Furthermore, by taking measurements of the SL signal, rather than DL exclusively, the dimensionality of the measurement vector is increased, effectively relaxing number of DLs required for localization. This begets a fully-determined (or overdetermined) system, when satellite clock parameters are estimated.

We advocate a new estimation paradigm, where cooperation over the SL is used to overcome the challenges of clock synchronization for LEO PNT. We propose a new algorithm, joint cooperative localization and synchronization (JCLS), which uses TOA measurements of the DL and SL signals to jointly estimate the values of clock offsets and UE position coordinates. The goals of this paper are: to derive the performance limits for JCLS using Fisher information and Cramér-Rao lower bound (CRLB) analysis; and demonstrate the feasibility of such an algorithm for 3GPP-compliant LCS in variable-size xG NTN without requiring GNSS or a gNB. Our simulation results demonstrate a mean 3D position error of 48 m for an NTN consisting of 2 UEs and 11 LEO satellites, which outperforms non-cooperative localization by 100%.

Notations: Random variables are displayed in sans serif, upright fonts; their realizations in serif, italic fonts. Vectors and matrices are denoted by bold lowercase and uppercase letters, respectively. For example, a random variable and its realization are denoted by x and x; a random vector and its realization are denoted by $\mathbf{x}$ and $\boldsymbol{x}$; a random matrix and its realization are denoted by $\mathbf{X}$ and $\boldsymbol{X}$, respectively. Sets and random sets are denoted by upright sans serif and calligraphic font, respectively. For example, a random set and its realization are denoted by X and $\mathcal{X}$, respectively. The m-by-n matrix of zeros (resp. ones) is denoted by $\mathbf{0}_{m\times n}$ (resp. $\mathbf{1}_{m\times n}$); when $n=1$, the m-dimensional vector of zeros (resp. ones) is simply denoted by $\mathbf{0}_m$ (resp. $\mathbf{1}_m$). The m-by-m identity matrix is denoted by $\boldsymbol{I}_m$: the subscript is removed when the dimension of the matrix is clear from the context. For a collection of vectors, $\boldsymbol{v}_i$, with $i\in\{1,2,\ldots,I\}$, the expanded column vector is denoted by $\boldsymbol{v}_{1:I}=\left[\,\boldsymbol{v}_1^{\mathrm{T}}\;\boldsymbol{v}_2^{\mathrm{T}}\;\cdots\;\boldsymbol{v}_I^{\mathrm{T}}\,\right]^{\mathrm{T}}$. For a collection of scalars, $a_{i,j}$, with $j\in\{1,2,\ldots,J\}$, the expanded column vector is denoted by $\boldsymbol{a}_{1:I,1:J}=\left[\,[\boldsymbol{a}_{1,1:J}]^{\mathrm{T}}\,[\boldsymbol{a}_{2,1:J}]^{\mathrm{T}}\;\cdots\;[\boldsymbol{a}_{I,1:J}]^{\mathrm{T}}\,\right]^{\mathrm{T}}$, with $\boldsymbol{a}_{i,1:J}=\left[\,a_{i,1}\;a_{i,2}\;\cdots\;a_{i,J}\,\right]^{\mathrm{T}}$. The euclidean L_2 norm of vector $\boldsymbol{v}$ is denoted by $||\boldsymbol{v}||_2$.

II. System Model

A. Network Setting

Consider an NTN that consists of N_{UE} UEs and N_{LEO} LEO satellites, where the satellites transmit reference signals for localization over the DL, and the UEs cooperate over the SL. Define $\mathcal{N}_{\mathrm{UE}}=\{1,2,\ldots,N_{\mathrm{UE}}\}$ and $\mathcal{N}_{\mathrm{LEO}}=\{1,2,\ldots,N_{\mathrm{LEO}}\}$ to be the index sets for UEs and satellites, respectively. The satellites transmit system information block (SIB)-19, which includes precise ephemerides from LEO satellites' unobstructed GNSS access, to the UEs. Each UE takes TOA measurements from the satellite DLs and simultaneously measures SL TOAs while sharing DL TOAs with other UEs. We describe the observation model according to $\boldsymbol{\rho}(\mathbf{n};\boldsymbol{\theta})=\boldsymbol{h}(\boldsymbol{\theta})+\mathbf{n}$, where $\boldsymbol{\rho}$ are the random TOA pseudorange measurements, $\boldsymbol{h}(\boldsymbol{\theta})$ are the synchronized TOA models as a function of network parameters, and $\mathbf{n}$ are the random TOA noises.

B. Synchronized TOA Model

Denote the known satellite positions as $\boldsymbol{s}_k=[\,x_k\;y_k\;z_k\,]^{\mathrm{T}}$ for all $k\in\mathcal{N}_{\mathrm{LEO}}$. Each satellite is synchronized for communication data links across inter-satellite links (ISLs), but has some unknown clock offset, θ_k^{LEO}. Each UE is considered stationary, positioned at $[\,\theta_i^{\mathrm{x}}\;\;\theta_i^{\mathrm{y}}\;\;\theta_i^{\mathrm{z}}\,]^{\mathrm{T}}$, with an unknown clock offset, θ_i^{δ}. Thus, we describe the state of each UE by $\boldsymbol{\theta}_i^{\mathrm{UE}}=[\,\theta_i^{\mathrm{x}}\;\theta_i^{\mathrm{y}}\;\theta_i^{\mathrm{z}}\;\theta_i^{\delta}\,]^{\mathrm{T}}$ for all $i\in\mathcal{N}_{\mathrm{UE}}$. We assume that θ_k^{LEO} and θ_i^{δ} are in units of km and are related to the clock offset in seconds by a factor of $\frac{c}{1000}$, where c is the speed of light in units of $\frac{m}{s}$. All satellite and UE positions are also in units of km. We define the vectors $\boldsymbol{\theta}^{\mathrm{LEO}}=\boldsymbol{\theta}^{\mathrm{LEO}}_{1:N_{\mathrm{LEO}}}$ and $\boldsymbol{\theta}^{\mathrm{UE}}=\boldsymbol{\theta}^{\mathrm{UE}}_{1:N_{\mathrm{UE}}}$. The network state can be described by the parameter vector $\boldsymbol{\theta}$:

$$\boldsymbol{\theta}=\left[\,\boldsymbol{\theta}^{\mathrm{LEO}\,\mathrm{T}}\;\boldsymbol{\theta}^{\mathrm{UE}\,\mathrm{T}}\,\right]^{\mathrm{T}} \tag{1}$$

Let every UE make TOA measurements from each satellite and assume that DL TOAs are broadcast from all other UEs to one master UE which will perform the JCLS estimation. Then, each UE will have N_{LEO} independent DL TOAs and $N_{\mathrm{UE}}-1$ independent SL TOAs. The TOAs are modeled in terms of known and unknown parameters:

$$h_{i,k}^{\mathrm{DL}}(\boldsymbol{\theta})=\left\|[\,\theta_i^{\mathrm{x}}\;\theta_i^{\mathrm{y}}\;\theta_i^{\mathrm{z}}\,]^{\mathrm{T}}-\boldsymbol{s}_k\right\|_2-\theta_i^{\delta}+\theta_k^{\mathrm{LEO}} \tag{2}$$

$$h_{i,j}^{\mathrm{SL}}(\boldsymbol{\theta})=\left\|[\,\theta_i^{\mathrm{x}}\;\theta_i^{\mathrm{y}}\;\theta_i^{\mathrm{z}}\,]^{\mathrm{T}}-[\,\theta_j^{\mathrm{x}}\;\theta_j^{\mathrm{y}}\;\theta_j^{\mathrm{z}}\,]^{\mathrm{T}}\right\|_2-\theta_i^{\delta}+\theta_j^{\delta} \tag{3}$$

Note that we assume deterministic, known satellite positions, but in cases where ephemerides are generated from two-line element (TLE) files and numerical propagation models, e.g., simplified general perturbation (SGP) propagators, the satellite positions must also be estimated [17]. We denote the DL and SL measurement model vectors as $\boldsymbol{h}^{\mathrm{DL}}(\boldsymbol{\theta})=\boldsymbol{h}^{\mathrm{DL}}_{1:N_{\mathrm{UE}},1:N_{\mathrm{LEO}}}(\boldsymbol{\theta})$ and $\boldsymbol{h}^{\mathrm{SL}}(\boldsymbol{\theta})=\boldsymbol{h}^{\mathrm{SL}}_{1:N_{\mathrm{UE}},1:N_{\mathrm{UE}}}(\boldsymbol{\theta})$. Thus, the collection of synchronized TOA models is

$$\boldsymbol{h}(\boldsymbol{\theta})=\left[\,\boldsymbol{h}^{\mathrm{DL}}(\boldsymbol{\theta})^{\mathrm{T}}\;\;\boldsymbol{h}^{\mathrm{SL}}(\boldsymbol{\theta})^{\mathrm{T}}\,\right]^{\mathrm{T}}. \tag{4}$$

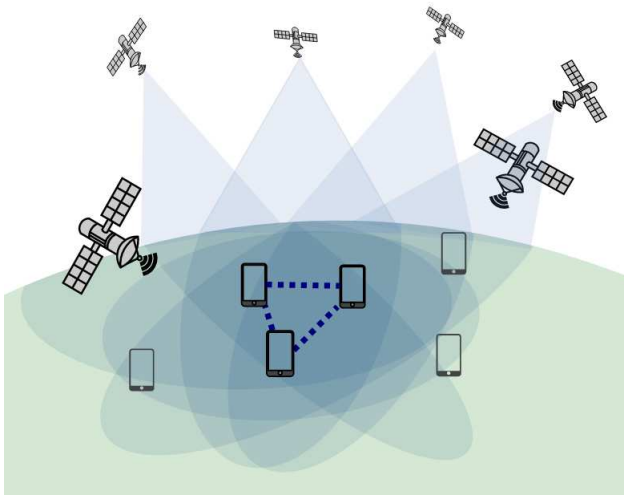

Fig. 1: UE cooperation over sidelinks and LEO downlinks. The 3 center UEs (in bold) have access to all downlinks and sidelinks and can perform joint cooperative localization and synchronization. The other UEs cannot localize themselves, because they are missing necessary downlinks.

C. Observation Model

For the DL between the ith UE and kth LEO satellite or the SL between the ith and jth UEs, the observation model for TOA measurements becomes:

$$\rho_{i,k}^{\mathrm{DL}} = h^{\mathrm{DL}}(\boldsymbol{\theta}_i^{\mathrm{UE}}, \theta_k^{\mathrm{LEO}}) + \mathsf{n}_{i,k}^{\mathrm{DL}} \tag{5a}$$

$$\rho_{i,j}^{\mathrm{SL}} = h^{\mathrm{SL}}(\boldsymbol{\theta}_i^{\mathrm{UE}}, \boldsymbol{\theta}_j^{\mathrm{UE}}) + \mathsf{n}_{i,j}^{\mathrm{SL}}. \tag{5b}$$

We define the DL and SL measurement vectors as $\boldsymbol{\rho}^{\mathrm{DL}} = \boldsymbol{\rho}^{\mathrm{DL}}_{1:N_{\mathrm{UE}},1:N_{\mathrm{LEO}}}$ and $\boldsymbol{\rho}^{\mathrm{SL}} = \boldsymbol{\rho}^{\mathrm{SL}}_{1:N_{\mathrm{UE}},1:N_{\mathrm{UE}}}$. Thus, the measurement vector is

$$\boldsymbol{\rho}(\mathbf{n};\boldsymbol{\theta}) = \boldsymbol{h}(\boldsymbol{\theta}) + \mathbf{n} \tag{6}$$

where $\mathbf{n}$ is the random vector of additive measurement noises. The errors for each measurement vary according to $\mathsf{n}_{i,k}^{\mathrm{DL}} \sim \mathcal{N}(0,\, {\sigma_{i,k}^{\mathrm{DL}}}^2)$ and $\mathsf{n}_{i,j}^{\mathrm{SL}} \sim \mathcal{N}(0,\, {\sigma_{i,j}^{\mathrm{SL}}}^2)$ for all $i,j \in \mathcal{N}_{\mathrm{UE}}$ and $k \in \mathcal{N}_{\mathrm{LEO}}$ such that $i \neq j$. Assume that the variance of ionosphere and troposphere delays are negligible relative to the receiver noises. Then, the DL and SL noise vectors are $\mathbf{n}^{\mathrm{DL}} = \mathbf{n}^{\mathrm{DL}}_{1:N_{\mathrm{UE}},1:N_{\mathrm{LEO}}}$ and $\mathbf{n}^{\mathrm{SL}} = \mathbf{n}^{\mathrm{SL}}_{1:N_{\mathrm{UE}},1:N_{\mathrm{UE}}}$. The noise vector is

$$\mathbf{n} = \begin{bmatrix} \mathbf{n}^{\mathrm{DL}\,\mathrm{T}} & \mathbf{n}^{\mathrm{SL}\,\mathrm{T}} \end{bmatrix}^{\mathrm{T}} \tag{7}$$

where the covariance matrix of $\mathbf{n}$ is defined as $\boldsymbol{\Sigma} \triangleq \mathbb{E}\{\mathbf{n}\mathbf{n}^{\mathrm{T}}\}$.

In Fig. 1, an example NTN provides $N_{\mathrm{UE}} = 3$ UEs PNT from $N_{\mathrm{LEO}} = 6$ LEO satellites. Cooperation between the UEs allows joint synchronization and localization (i.e., estimation of both clock offset and position parameters).

III. Fisher Information Analysis

According to the information inequality, the mean square error (MSE) is bounded by the inverse of the Fisher information matrix (FIM):

$$\mathbb{E}_{\boldsymbol{\rho}}\left\{ ||\hat{\boldsymbol{\theta}} - \boldsymbol{\theta}||_2^2 \right\} \geqslant \mathrm{tr}\left\{ \boldsymbol{F}(\boldsymbol{\theta})^{-1} \right\}. \tag{8}$$

A. CRLB Regularity Condition

Note that the joint probability density function of $\boldsymbol{\rho}$, $f_{\boldsymbol{\rho}}(\boldsymbol{\rho};\boldsymbol{\theta})$, meets the regularity condition in [18], and we will be able to calculate the CRLB:

$$\mathbb{E}_{\boldsymbol{\rho}}\{\nabla_{\boldsymbol{\theta}} \ln f_{\boldsymbol{\rho}}(\boldsymbol{\rho};\boldsymbol{\theta})\} = \mathbf{0} \tag{9}$$

In the presence of Gaussian noise,

$$\begin{aligned} \ln f_{\boldsymbol{\rho}}(\boldsymbol{\rho};\boldsymbol{\theta}) &= \ln \prod_{i\in\mathcal{N}_{\mathrm{UE}}} \prod_{k\in\mathcal{N}_{\mathrm{LEO}}} f_{\boldsymbol{\rho}}(\rho_{i,k}^{\mathrm{DL}};\boldsymbol{\theta}) \\ &\quad \times \prod_{j\in\mathcal{N}_{\mathrm{UE}}\setminus\{i\}} f_{\boldsymbol{\rho}}(\rho_{i,j}^{\mathrm{SL}};\boldsymbol{\theta}) \\ &= \frac{1}{2} \sum_{i\in\mathcal{N}_{\mathrm{UE}}} \sum_{k\in\mathcal{N}_{\mathrm{LEO}}} \frac{(\rho_{i,k}^{\mathrm{DL}} - h_{i,k}^{\mathrm{DL}})^2}{-{\sigma_{i,k}^{\mathrm{DL}}}^2} \\ &\quad + \sum_{j\in\mathcal{N}_{\mathrm{UE}}\setminus\{i\}} \frac{(\rho_{i,j}^{\mathrm{SL}} - h_{i,j}^{\mathrm{SL}})^2}{-{\sigma_{i,j}^{\mathrm{SL}}}^2} \\ &= -\frac{1}{2} \boldsymbol{r}(\boldsymbol{\rho};\boldsymbol{\theta})^{\mathrm{T}} \boldsymbol{\Sigma}^{-1} \boldsymbol{r}(\boldsymbol{\rho};\boldsymbol{\theta}) \end{aligned} \tag{10}$$

where the residual vector is $\boldsymbol{r}(\boldsymbol{\rho};\boldsymbol{\theta}) = \boldsymbol{\rho} - \boldsymbol{h}(\boldsymbol{\theta})$, and $\mathbb{E}_{\boldsymbol{\rho}}\{\boldsymbol{r}(\boldsymbol{\rho};\boldsymbol{\theta})\} = \boldsymbol{h}(\boldsymbol{\theta}) - \boldsymbol{h}(\boldsymbol{\theta}) = \mathbf{0}$ in zero-mean noise. Then, the score function of $f_{\boldsymbol{\rho}}(\boldsymbol{\rho};\boldsymbol{\theta})$ is defined as

$$\begin{aligned} \boldsymbol{u}_{\boldsymbol{\rho}}(\boldsymbol{\rho};\boldsymbol{\theta}) &\triangleq \nabla_{\boldsymbol{\theta}} \ln f_{\boldsymbol{\rho}}(\boldsymbol{\rho};\boldsymbol{\theta}) \\ &= \boldsymbol{J}_{\boldsymbol{h}}(\boldsymbol{\theta})^{\mathrm{T}} \boldsymbol{\Sigma}^{-1} \boldsymbol{r}(\boldsymbol{\rho};\boldsymbol{\theta}) \end{aligned} \tag{11}$$

where the measurement Jacobian is defined as $\boldsymbol{J}_{\boldsymbol{h}}(\boldsymbol{\theta}) \triangleq \nabla_{\boldsymbol{\theta}} \boldsymbol{h}(\boldsymbol{\theta})$. Finally, we see that the regulatory condition is met:

$$\begin{aligned} \mathbb{E}_{\boldsymbol{\rho}}\{\boldsymbol{u}_{\boldsymbol{\rho}}(\boldsymbol{\rho};\boldsymbol{\theta})\} &= \boldsymbol{J}_{\boldsymbol{h}}(\boldsymbol{\theta})^{\mathrm{T}} \boldsymbol{\Sigma}^{-1} \mathbb{E}_{\boldsymbol{\rho}}\{\boldsymbol{r}(\boldsymbol{\rho};\boldsymbol{\theta})\} \\ &= \mathbf{0} \end{aligned} \tag{12}$$

B. FIM Derivation

The Hessian of $f_{\boldsymbol{\rho}}(\boldsymbol{\rho};\boldsymbol{\theta})$ is defined as

$$\boldsymbol{H}_{\boldsymbol{\rho}}(\boldsymbol{\rho};\boldsymbol{\theta}) \triangleq \nabla_{\boldsymbol{\theta}} \boldsymbol{u}_{\boldsymbol{\rho}}(\boldsymbol{\rho};\boldsymbol{\theta}) \tag{13a}$$

$$= \nabla_{\boldsymbol{\theta}}^2 \ln f_{\boldsymbol{\rho}}(\boldsymbol{\rho};\boldsymbol{\theta}). \tag{13b}$$

The FIM of $\boldsymbol{\theta}$ is given by expectation over $\boldsymbol{H}_{\boldsymbol{\rho}}(\boldsymbol{\rho};\boldsymbol{\theta})$:

$$\begin{aligned} \boldsymbol{F}_{\boldsymbol{\theta}} &\triangleq -\mathbb{E}_{\boldsymbol{\rho}}\{\boldsymbol{H}_{\boldsymbol{\rho}}(\boldsymbol{\rho};\boldsymbol{\theta})\} \\ &= -\mathbb{E}_{\boldsymbol{\rho}}\{\nabla_{\boldsymbol{\theta}} \boldsymbol{r}(\boldsymbol{\rho};\boldsymbol{\theta})^{\mathrm{T}} \boldsymbol{\Sigma}^{-1} \boldsymbol{J}_{\boldsymbol{h}}(\boldsymbol{\theta})\} \\ &= -\mathbb{E}_{\boldsymbol{\rho}}\{-\boldsymbol{J}_{\boldsymbol{h}}(\boldsymbol{\theta})^{\mathrm{T}} \boldsymbol{\Sigma}^{-1} \boldsymbol{J}_{\boldsymbol{h}}(\boldsymbol{\theta}) + \boldsymbol{r}(\boldsymbol{\rho};\boldsymbol{\theta})^{\mathrm{T}} \boldsymbol{\Sigma}^{-1} \boldsymbol{H}_{\boldsymbol{h}}(\boldsymbol{\theta})\} \\ &= \boldsymbol{J}_{\boldsymbol{h}}(\boldsymbol{\theta})^{\mathrm{T}} \boldsymbol{\Sigma}^{-1} \boldsymbol{J}_{\boldsymbol{h}}(\boldsymbol{\theta}) \end{aligned} \tag{14}$$

where $\boldsymbol{H}_{\boldsymbol{h}}(\boldsymbol{\theta}) \triangleq \nabla_{\boldsymbol{\theta}}^2 \boldsymbol{h}(\boldsymbol{\theta})$ is the Hessian of $\boldsymbol{h}(\boldsymbol{\theta})$. Now, we have that $\boldsymbol{J}_{\boldsymbol{h}}(\boldsymbol{\theta})^{\mathrm{T}} \boldsymbol{\Sigma}^{-1} \boldsymbol{J}_{\boldsymbol{h}}(\boldsymbol{\theta}) \succcurlyeq \mathbf{0}$ (that is, $\boldsymbol{F}_{\boldsymbol{\theta}}$ is positive semidefinite), and by the information inequality, the MSE is bounded by

$$\mathbb{E}_{\boldsymbol{\rho}}\left\{ ||\boldsymbol{\theta} - \hat{\boldsymbol{\theta}}||_2^2 \right\} \geqslant \mathrm{Tr}\{(\boldsymbol{J}_{\boldsymbol{h}}(\boldsymbol{\theta})^{\mathrm{T}} \boldsymbol{\Sigma}^{-1} \boldsymbol{J}_{\boldsymbol{h}}(\boldsymbol{\theta}))^{-1}\}. \tag{15}$$

IV. Joint Cooperative Localization and Synchronization Algorithm

We describe the maximum likelihood estimation (MLE) problem for JCLS, propose an algorithm for estimating $\boldsymbol{\theta}$, and derive the requisite Jacobian matrix, $\boldsymbol{J}_{\boldsymbol{h}}(\boldsymbol{\theta})$, for iteratively solving the approximate optimization problem.

A. Problem Formulation

The MLE problem for JCLS is defined as (16a). In the presence of independent Gaussian noise, by (10), the MLE problem is equivalent to the weighted nonlinear least squares (WNLS) problem:

$$\hat{\boldsymbol{\theta}} \triangleq \arg\max_{\boldsymbol{\theta}} L_{\boldsymbol{\rho}}(\boldsymbol{\theta}) \tag{16a}$$

$$= \arg\max_{\boldsymbol{\theta}} f_{\boldsymbol{\rho}}(\boldsymbol{\rho};\boldsymbol{\theta})$$

$$= \arg\min_{\boldsymbol{\theta}} \boldsymbol{r}(\boldsymbol{\rho};\boldsymbol{\theta})^{\mathrm{T}} \boldsymbol{\Sigma}^{-1} \boldsymbol{r}(\boldsymbol{\rho};\boldsymbol{\theta}). \tag{16b}$$

Note that $\boldsymbol{\theta} \in \mathbb{R}^{N_{\mathrm{LEO}}+4N_{\mathrm{UE}}}$ and $\boldsymbol{\rho} \in \mathbb{R}^{N_{\mathrm{UE}}(N_{\mathrm{UE}}+N_{\mathrm{LEO}}-1)}$, therefore consider

$$N_{\mathrm{LEO}} + 4N_{\mathrm{UE}} \leqslant N_{\mathrm{UE}}(N_{\mathrm{UE}} + N_{\mathrm{LEO}} - 1) \tag{17}$$

which is satisfied, for example, by $N_{\mathrm{UE}} = 2, N_{\mathrm{LEO}} = 6$. The function $-L_{\boldsymbol{\rho}}(\boldsymbol{\theta})$ is convex if and only if $-\boldsymbol{H}_{\boldsymbol{\rho}}(\boldsymbol{\rho};\boldsymbol{\theta}) \succcurlyeq \mathbf{0}$ (13b). However, we see that by (14), convexity holds if

$$\boldsymbol{J}_{\boldsymbol{h}}(\hat{\boldsymbol{\theta}})^{\mathrm{T}} \boldsymbol{\Sigma}^{-1} \boldsymbol{J}_{\boldsymbol{h}}(\hat{\boldsymbol{\theta}}) \succcurlyeq \boldsymbol{r}(\boldsymbol{\rho};\hat{\boldsymbol{\theta}})^{\mathrm{T}} \boldsymbol{\Sigma}^{-1} \boldsymbol{H}_{\boldsymbol{h}}(\hat{\boldsymbol{\theta}}) \tag{18}$$

which is generally not met for large $||\boldsymbol{\theta} - \hat{\boldsymbol{\theta}}||_2$, which cause large $\boldsymbol{r}(\boldsymbol{\rho};\hat{\boldsymbol{\theta}})$.

B. JCLS Algorithm

We propose a two-step JCLS algorithm using the Gauss-Newton (GN) and Levenberg-Marquardt (LM) methods to solve the non-convex problem in (16b). In step 1, we solve the joint localization problem without clock synchronization to avoid local minima and reach a rough parameter estimate. We perform step 1 using the GN method to converge quickly without computing $\boldsymbol{H}_{\boldsymbol{h}}(\hat{\boldsymbol{\theta}})$. In step 2, the clock parameters are introduced and the step 1 estimate is refined to jointly localize and synchronize. In order to handle large $N_{\mathrm{LEO}} + 4N_{\mathrm{UE}}$, we base step 2 on LM, which offers numerical robustness through matrix regularization. That is, we leverage the fast convergence of GN and the numerical robustness of LM in our JCLS algorithm.

1) GN Step: We solve the problem

$$\arg\min_{\boldsymbol{\theta}^{\mathrm{UE}}} \boldsymbol{r}\left(\boldsymbol{\rho}; \begin{bmatrix}\mathbf{0}_{N_{\mathrm{LEO}}} \\ \boldsymbol{\theta}^{\mathrm{UE}}\end{bmatrix}\right)^{\mathrm{T}} \boldsymbol{\Sigma}^{-1} \boldsymbol{r}\left(\boldsymbol{\rho}; \begin{bmatrix}\mathbf{0}_{N_{\mathrm{LEO}}} \\ \boldsymbol{\theta}^{\mathrm{UE}}\end{bmatrix}\right)$$

using the GN method. The GN method approximates the objective function locally around the current parameter estimate using a first-order Taylor expansion. It uses $\boldsymbol{J}_{\boldsymbol{h}}$ to infer local curvature information which is used to scale step-size, improving convergence without requiring the calculation of $\boldsymbol{H}_{\boldsymbol{h}}(\hat{\boldsymbol{\theta}})$. Instead it approximates the Hessian by

$$\tilde{\boldsymbol{H}}_{\boldsymbol{h}}^{\mathrm{GN}}(\hat{\boldsymbol{\theta}}) = \boldsymbol{J}_{\boldsymbol{h}}(\hat{\boldsymbol{\theta}})^{\mathrm{T}} \boldsymbol{\Sigma}^{-1} \boldsymbol{J}_{\boldsymbol{h}}(\hat{\boldsymbol{\theta}}). \tag{19}$$

Furthermore, we exclude the clock parameters from $\hat{\boldsymbol{\theta}}$ to ensure matrix invertibility and proceed using the update equation

$$\hat{\boldsymbol{\theta}}_{n+1} = \hat{\boldsymbol{\theta}}_n + \left(\tilde{\boldsymbol{H}}_{\boldsymbol{h}}^{\mathrm{GN}}(\hat{\boldsymbol{\theta}})\right)^{-1} \boldsymbol{J}_{\boldsymbol{h}}(\hat{\boldsymbol{\theta}}_n)^{\mathrm{T}} \boldsymbol{\Sigma}^{-1} \boldsymbol{r}(\boldsymbol{\rho}, \hat{\boldsymbol{\theta}}_n) \tag{20}$$

until the stopping criterion, $\frac{||\hat{\boldsymbol{\theta}}_{n+1} - \hat{\boldsymbol{\theta}}_n||}{||\hat{\boldsymbol{\theta}}_{n+1}||}$, is sufficiently small.

2) LM Step: We solve the probem in (16b) using the LM method. Though it converges more slowly than GN, the LM algorithm enables joint estimation of clock and position parameters by regularizing the Hessian approximation,

$$\tilde{\boldsymbol{H}}_{\boldsymbol{h}}^{\mathrm{LM}}(\hat{\boldsymbol{\theta}}) = \boldsymbol{J}_{\boldsymbol{h}}(\hat{\boldsymbol{\theta}})^{\mathrm{T}} \boldsymbol{\Sigma}^{-1} \boldsymbol{J}_{\boldsymbol{h}}(\hat{\boldsymbol{\theta}}) + \lambda \boldsymbol{I} \tag{21}$$

for some carefully selected λ. For large values of λ, LM behaves like gradient descent, taking small linear steps in the direction of steepest descent. Conversely, for small values of λ, the algorithm behaves more like the Gauss-Newton method, taking larger, more direct steps towards the minimum. After the GN step has terminated, $\hat{\boldsymbol{\theta}}$ is updated to include clock parameters, and we proceed according to the algorithm in [19].

The Jacobian $\boldsymbol{J}_{\boldsymbol{h}}$, must be calculated for both steps of the JCLS algorithm. From the structures of the vectors in (2) and (4), partition $\boldsymbol{J}_{\boldsymbol{h}}$ as:

$$\boldsymbol{J}_{\boldsymbol{h}}(\boldsymbol{\theta}) = \left[\begin{array}{c|c} \boldsymbol{A}_{N_{\mathrm{UE}}N_{\mathrm{LEO}} \times N_{\mathrm{LEO}}} & \boldsymbol{B}_{N_{\mathrm{UE}}N_{\mathrm{LEO}} \times 4N_{\mathrm{UE}}} \\ \hline \mathbf{0}_{N_{\mathrm{UE}}^2 - N_{\mathrm{UE}} \times N_{\mathrm{LEO}}} & \boldsymbol{C}_{N_{\mathrm{UE}}^2 - N_{\mathrm{UE}} \times 4N_{\mathrm{UE}}} \end{array}\right] \tag{22}$$

where

$$\boldsymbol{A} = \frac{\partial \boldsymbol{h}^{\mathrm{DL}}}{\partial \boldsymbol{\theta}^{\mathrm{LEO}^{\mathrm{T}}}} = \left[\boldsymbol{I}_K \overset{\times N_{\mathrm{UE}}}{\cdots\cdots}\right]^{\mathrm{T}} \tag{23}$$

$$\boldsymbol{B} = \frac{\partial \boldsymbol{h}^{\mathrm{DL}}}{\partial \boldsymbol{\theta}^{\mathrm{UE}^{\mathrm{T}}}} = \begin{bmatrix} \frac{\partial \boldsymbol{h}^{\mathrm{DL}}}{\partial \boldsymbol{\theta}_1^{\mathrm{UE}}} & \mathbf{0} & \dots & \mathbf{0} \\ \mathbf{0} & \ddots & \ddots & \vdots \\ \vdots & \ddots & \ddots & \mathbf{0} \\ \mathbf{0} & \dots & \mathbf{0} & \frac{\partial \boldsymbol{h}^{\mathrm{DL}}}{\partial \boldsymbol{\theta}_{N_{\mathrm{UE}}}^{\mathrm{UE}}} \end{bmatrix} \tag{24}$$

$$\boldsymbol{C} = \frac{\partial \boldsymbol{h}^{\mathrm{SL}}}{\partial \boldsymbol{\theta}^{\mathrm{UE}^{\mathrm{T}}}} = \left[\frac{\partial \boldsymbol{h}_{1:N_{\mathrm{UE}},1:N_{\mathrm{UE}}}}{\partial \boldsymbol{\theta}_{1:N_{\mathrm{UE}}}^{\mathrm{T}}}\right] \tag{25}$$

with derivatives:

$$\frac{\partial \boldsymbol{h}_{i,k}^{\mathrm{DL}}}{\partial \boldsymbol{\theta}_i^{\mathrm{UE}^{\mathrm{T}}}} = \left[\frac{\theta_i^{\mathrm{x}} - s_k^{\mathrm{x}}}{||\boldsymbol{\theta}_i^{\mathrm{UE}} - \boldsymbol{s}_{\boldsymbol{k}}||_2} \; \frac{\theta_i^{\mathrm{y}} - s_k^{\mathrm{y}}}{||\boldsymbol{\theta}_i^{\mathrm{UE}} - \boldsymbol{s}_{\boldsymbol{k}}||_2} \; \frac{\theta_i^{\mathrm{z}} - s_k^{\mathrm{z}}}{||\boldsymbol{\theta}_i^{\mathrm{UE}} - \boldsymbol{s}_{\boldsymbol{k}}||_2} \; 1\right]$$

$$\frac{\partial \boldsymbol{h}^{\mathrm{DL}}}{\partial \boldsymbol{\theta}_i^{\mathrm{UE}^{\mathrm{T}}}} = \left[\frac{\partial \boldsymbol{h}_{i,1:N_{\mathrm{LEO}}}^{\mathrm{DL}}}{\partial \boldsymbol{\theta}_i^{\mathrm{UE}}}^{\mathrm{T}}\right]^{\mathrm{T}} \tag{26}$$

$$d_{i,j} = ||\,[\theta_i^x \; \theta_i^y \; \theta_i^z\,]^{\mathrm{T}} - [\theta_j^x \theta_j^y \theta_j^z]^{\mathrm{T}}||_2$$

$$\frac{\partial h_{i,j}}{\partial \boldsymbol{\theta}_l} = \begin{cases} [\,\frac{x_i - x_j}{d_{i,j}} \; \frac{y_i - y_j}{d_{i,j}} \; \frac{z_i - z_j}{d_{i,j}} \; 1\,]^{\mathrm{T}} & \text{for } i = l \\ -[\,\frac{x_i - x_j}{d_{i,j}} \; \frac{y_i - y_j}{d_{i,j}} \; \frac{z_i - z_j}{d_{i,j}} \; 1\,]^{\mathrm{T}} & \text{for } j = l \\ \mathbf{0}_4 & \text{otherwise} \end{cases}$$

C. 3GPP-Compliant NTN Settings

Using MATLAB R2023a and the Satellite Communications Toolbox, we simulate UEs receiving DLs from visible satellites and SLs from other UEs. We used the TLE files corresponding to the positions of the Starlink constellation on 10/22/2023 at 17:00:00.

The simulated signals are generated according to the methodology outlined in Sec. II, using 3GPP signal parameters as specified in [20] and [21]. Specifically, we assume that the

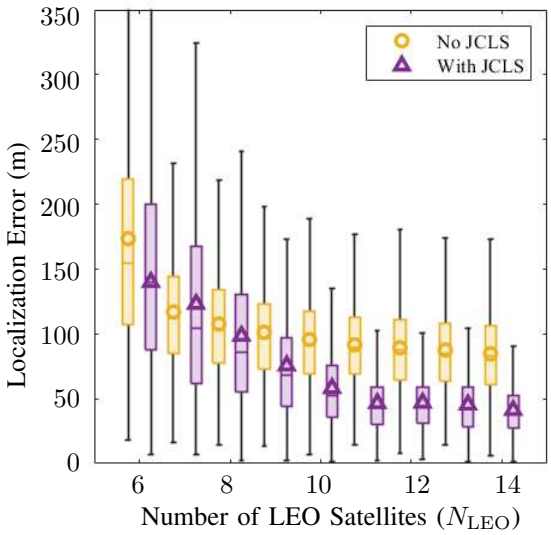

Fig. 2: Effect of Additional Downlinks on Localization Error ($N_{\mathrm{UE}} = 2$)

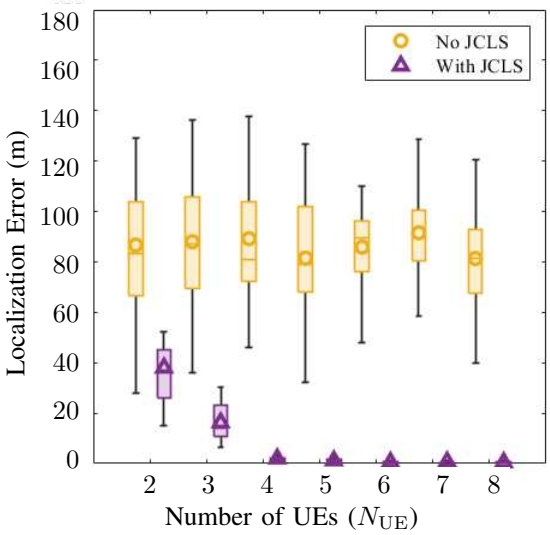

Fig. 3: Effect of Additional Sidelinks on Localization Error ($N_{\mathrm{LEO}} = 14$)

DL signal is transmitted over channel n512, which operates within the 3GPP NTN frequency range 2 (Ka-band) with a bandwidth of 200 MHz and an SNR of 0 dB. The SL signal has a bandwidth of 40 MHz and an SNR of 5 dB. The noise variance is determined by the signal propagation speed c, bandwidth β, and SNR γ. We use the CRLB for TOA error to calculate the minimum variances:

$$\sigma^2 = \frac{c^2}{8\left(\pi\beta\right)^2\gamma} \tag{27}$$

Consequently, the corresponding standard deviations of the ranging errors are $\sigma_{\mathrm{DL}} = 0.0001687$ km and $\sigma_{\mathrm{SL}} = 0.0003795$ km for the DL and SL signals, respectively.

In Fig. 2, the mean absolute error (MAE) per UE (that is, the average 3D position error), is shown for two UEs performing JCLS, compared to independent localization without synchronization for a varying number of satellite DLs. The master UE's position is fixed outside of the MIT Stata center. The other is randomly placed according to a uniform distribution with a circular radius of 0 to 500 m. We see that for this satellite geometry, the independent estimation method saturates at $N_{\mathrm{LEO}} = 7$ satellites, whereas JCLS saturates at $N_{\mathrm{LEO}} = 11$, leading to a 50% reduction in MAE for $N_{\mathrm{LEO}} \geqslant 11$.

In Fig. 3, the effect of adding additional UEs for $N_{\mathrm{LEO}} = 14$ is shown. We see that more UEs helps to improve localization accuracy beyond the saturation point in Fig. 2. However, the computation required for joint estimation with many UEs makes it difficult to converge on a solution with equal numbers of satellites and UEs. With $N_{\mathrm{LEO}} = 14$ and $N_{\mathrm{UE}} \geqslant 9$, JCLS reaches meter-level positioning accuracy.

D. Localization Performance by Bandwidth

In order to inform future NTN specifications (including bandwidth selection), we investigate the effect of changing DL and SL bandwidths on the localization accuracy. Fig. 4, shows that the localization root-mean-square error (RMSE) is tight with the CRLB for DL bandwidths greater than 40 MHz. Furthermore, the RMSE decreases as bandwith increases logarithmically. In Fig. 5, however, any SL bandwidth between $15 - 90$ MHz is acceptable for localization. Furthermore, both small and largeSL bandwidth (not pictured) exacerbate the nonlinearities of the SL TOA measurement and cause divergence with the proposed JCLS algorithm.

V. Conclusion

The proposed joint cooperative localization and synchronization strategy leverages cooperation over the sidelink to achieve PNT from LEO DLs that is sufficient for 3GPP LCS. With 10 satellites, even two UEs can achieve sub-50 m 3D positioning accuracy in a single time-step with 2 UEs or meter-level positioning accuracy with 9 UEs. Compared to non-cooperative estimation, JCLS asymptotically approaches a 100% improvement in high SNR regimes with 2 UEs. Thus, the sidelink will be crucial for both V2X and worldwide PNT in GNSS-denied environments. Performing clock synchronization jointly with localization increases the dimensionality of $\boldsymbol{J_h}(\boldsymbol{\theta})$. This makes applying traditional WNLS solution algorithms, such as GN, difficult. Through careful regularization, we can overcome that challenge and jointly estimate small clock drifts and large propagation times. Furthermore, by allowing cooperation between UEs, we increase the number of measurements available to the estimation algorithm, which enables over-constrained static estimation of location and

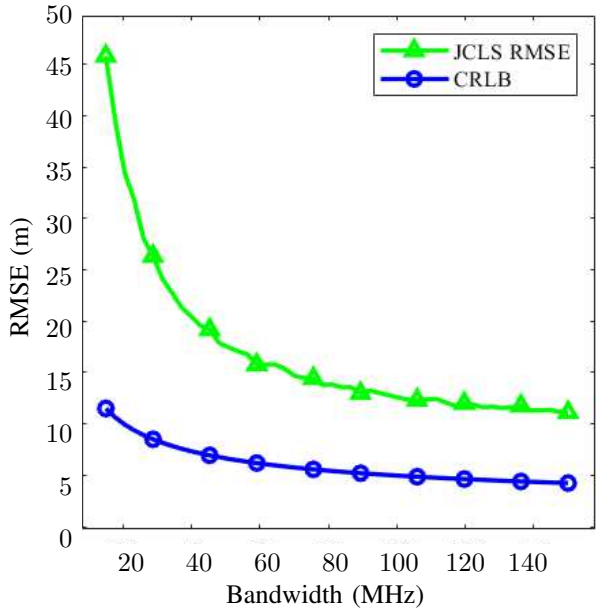

Fig. 4: Effect of DL Bandwidth on JCLS RMSE and CRLB: ($N_{\mathrm{UE}} = 14, N_{\mathrm{LEO}} = 3$)

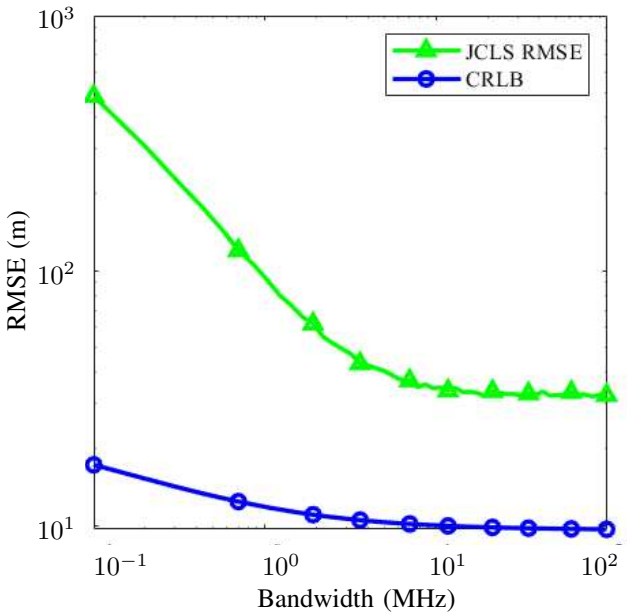

Fig. 5: Effect of SL Bandwidth on JCLS MSE and CRLB: ($N_{\mathrm{UE}} = 14, N_{\mathrm{LEO}} = 3$)

clock parameters and relaxes the requirement for 8 satellites in Doppler models to 5 satellites, when 3 UEs are available.

REFERENCES

[1] *Technical Specification Group Services and System Aspects; Location Services (LCS); Service description; Stage 1*, 3rd Generation Partnership Project 3GPP™ TS 22.071 V18.0.1 (2024-04), Apr. 2024, release 18.

[2] A. Conti, F. Morselli, Z. Liu, S. Bartoletti, S. Mazuelas, W. C. Lindsey, and M. Z. Win, "Location awareness in beyond 5G networks," *IEEE Commun. Mag.*, vol. 59, no. 11, pp. 22–27, Nov. 2021, special issue on *Location Awareness for 5G and Beyond*.

[3] *Technical Specification Group Services and System Aspects; Service requirements for the 5G system; Stage 1*, 3rd Generation Partnership Project 3GPP™ TR 22.261 V19.6.0 (2024-03), Mar. 2024, release 19.

[4] X. Lin, Z. Lin, S. E. Löwenmark, J. Rune, R. Karlsson, and Ericsson, "Doppler Shift Estimation in 5G New Radio Non-Terrestrial Networks," in *Proc. IEEE Global Telecomm. Conf.*, 2021, pp. 1–6.

[5] L. Chiaraviglio, S. Rossetti, S. Saida, S. Bartoletti, and N. Blefari-Melazzi, "Pencil beamforming increases human exposure to electromagnetic fields: True or false?" *IEEE Access*, vol. 9, pp. 25 158–25 171, 2021.

[6] S.-W. Ko, H. Chae, K. Han, S. Lee, D.-W. Seo, and K. Huang, "V2X-based vehicular positioning: Opportunities, challenges, and future directions," *IEEE Wireless Commun.*, vol. 28, no. 2, pp. 144–151, 2021.

[7] *The Department of the Air Force Role in Joint All-Domain Operations*, AFDP 3-99, Chief of Staff of the Air Force, Washington, DC, USA, 2021.

[8] M. Z. Win, Y. Shen, and W. Dai, "A theoretical foundation of network localization and navigation," *Proc. IEEE*, vol. 106, no. 7, pp. 1136–1165, Jul. 2018, special issue on *Foundations and Trends in Localization Technologies*.

[9] G. X. Gao, M. Sgammini, M. Lu, and N. Kubo, "Protecting GNSS receivers from jamming and interference," *Proc. IEEE*, vol. 104, no. 6, pp. 1327–1338, 2016.

[10] Z. Kassas, J. Khalife, M. Neinavaie, and T. Mortlock, "Opportunity comes knocking: overcoming GPS vulnerabilities with other satellites' signals," *Inside Unmanned Syst. Mag.*, pp. 30–35, 2020.

[11] K. Wang and A. El-Mowafy, "LEO satellite clock analysis and prediction for positioning applications," *Geo-spatial Inform. Sci.*, vol. 25, no. 1, pp. 14–33, 2022.

[12] C. T. Ardito, J. J. Morales, J. Khalife, A. Abdallah, Z. M. Kassas *et al.*, "Performance evaluation of navigation using LEO satellite signals with periodically transmitted satellite positions," in *Proc. Int. Technical Meeting of The Inst. of Navigation*, 2019, pp. 306–318.

[13] J. Khalife, M. Neinavaie, and Z. M. Kassas, "Navigation With Differential Carrier Phase Measurements From Megaconstellation LEO Satellites," in *Proc. IEEE Position Location and Navig. Symp.*, 2020, pp. 1393–1404.

[14] M. L. Psiaki, "Navigation using carrier doppler shift from a LEO constellation: TRANSIT on steroids," *Navigation*, vol. 68, no. 3, pp. 621–641, 2021.

[15] R. Sabbagh and Z. M. Kassas, "Observability analysis of receiver localization via pseudorange measurements from a single LEO satellite," *IEEE Control Syst. Lett.*, vol. 7, pp. 571–576, 2023.

[16] M. Z. Win, A. Conti, S. Mazuelas, Y. Shen, W. M. Gifford, D. Dardari, and M. Chiani, "Network localization and navigation via cooperation," *IEEE Commun. Mag.*, vol. 49, no. 5, pp. 56–62, May 2011.

[17] Z. Kassas, J. Morales, and J. Khalife, "New-age satellite-based navigation–STAN: simultaneous tracking and navigation with LEO satellite signals," *Inside GNSS Mag.*, vol. 14, no. 4, pp. 56–65, 2019.

[18] S. M. Kay, *Fundamentals of Statistical Signal Processing: Estimation Theory*. Prentice Hall, 1993.

[19] C. Mensing and S. Plass, "Positioning Algorithms for Cellular Networks Using TDOA," in *Proc. IEEE Int. Conf. Acoustics, Speech, and Signal Process.*, vol. 4, 2006, pp. IV–IV.

[20] *Technical Specification Group Radio Access Network; Solutions for NR to support non-terrestrial networks (NTN): Non-terrestrial networks (NTN) related RF and co-existence aspects*, 3rd Generation Partnership Project 3GPP™ TR 38.863 V18.1.0 (2024-03), Mar. 2024, release 18.

[21] *Technical Specification Group Radio Access Network; Solutions for NR to support non-terrestrial networks (NTN)*, 3rd Generation Partnership Project 3GPP™ TR 38.821 V16.2.0 (2023-03), Mar. 2023, release 16.